

CHAPTER 6

Particle Formation during Precipitation- Stripping

Recovery of Copper and Zinc from Brass Rinse Waters

Precipitation stripping (PS) is a unique technique of regeneration of metal loaded organic phase wherein the metal components extracted in the organic phase are precipitated out as an insoluble salt. It differs from conventional stripping in the sense, that the end product in this case is a precipitate of a sparingly soluble metal salt whereas, in conventional stripping it is a soluble metal salt in a strong mineral acid solution. In conventional stripping the metal dissolved in the mineral acid needs to be further reclaimed by electrowinning while in precipitation stripping the precipitates can find direct use or they can be converted to metal oxides by calcinations (Figure 6.1). PS is not a widely investigated area because the metal recovery is in the form of oxalates and oxides instead of the metal itself which may not be an attractive proposition for waste processors dealing with large capacities. Nevertheless, PS is an attractive tool that has the potential to generate revenue while cleaning up the targeted waste aqueous stream.

Metal recovery from waste streams using PS for reclamation has been a key aspect of this investigation. The recovery of copper from acidic chloride pickle liquors and ammoniacal spent etching solution was attained by PS. Zinc was also recovered from chloride pickle liquors using this technique. Considering the overall simplicity of this technique and the potential of this method for value added recovery of heavy metals makes PS a worthy candidate for detailed investigation. In this Chapter, brass rinse liquors were used as the metal source and precipitation during stripping of metal loaded organic phase is studied over wide range parametric variations to gain insights in particle formation behavior.

6.1 Summary of Literature

Precipitation-stripping is a three step process (i) Mass transfer of the complexed metal from the bulk organic phase to the oil-aqueous interface, (ii) Stripping of the metal ions, (iii) Mass transfer of metal ions in the aqueous phase and reaction with the oxalate ions (Konishi *et al.*, 1993). It is a combined process of stripping and precipitation stages, wherein oxalic acid acts

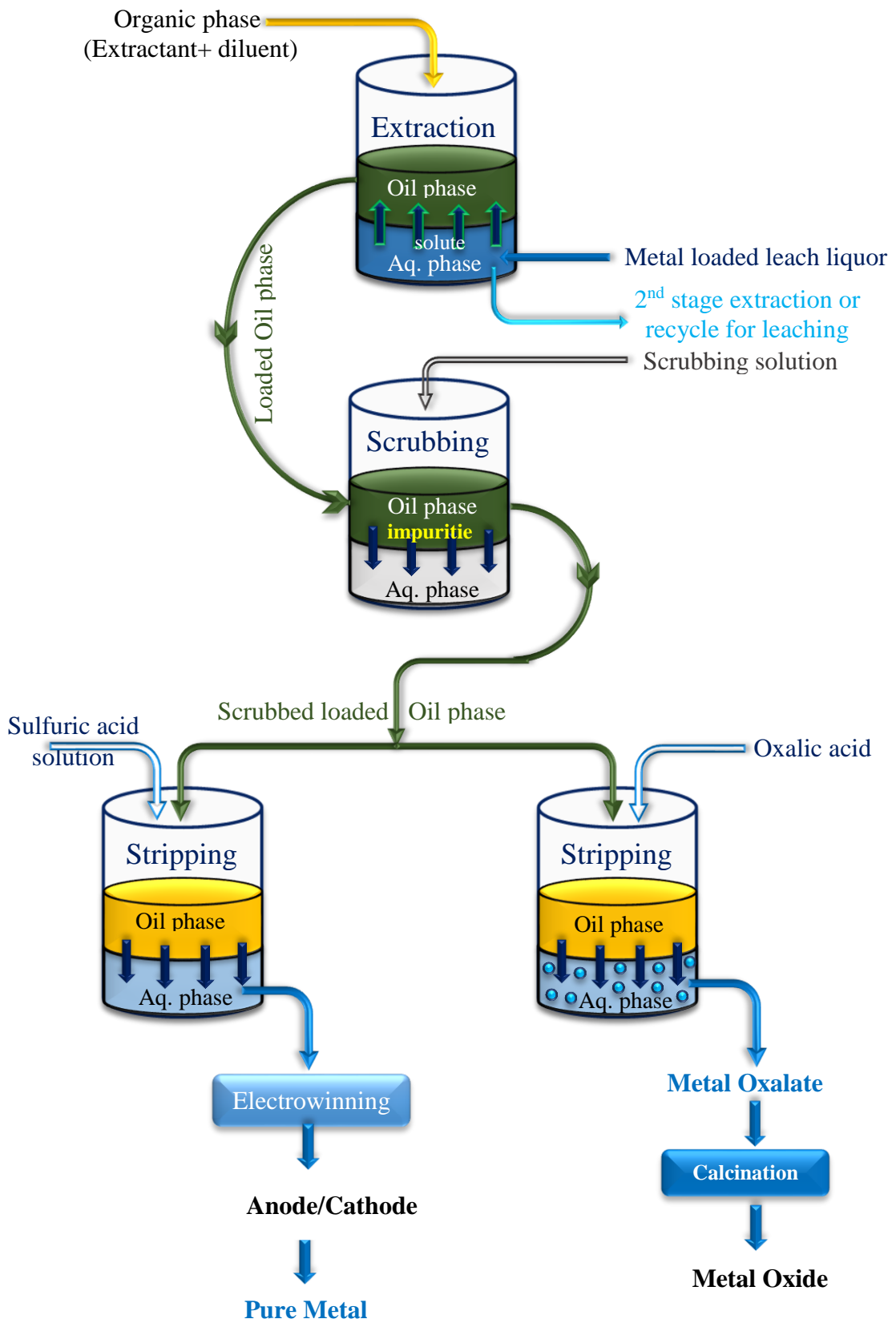


Fig.6.1: Ways to recover metal from aqueous stream

both as stripping and a precipitating agent. The metal gets stripped by hydrogen ions and is subsequently precipitated by oxalate anions (Konishi *et al.*, 1998) forming a sparingly soluble metal oxalate in aqueous media. H^+ ion is the driving force in stripping rather than the oxalate and the driving force by the oxalate ion itself is low (Campbell, 1999).

Equal organic to aqueous volumes is optimal in stripping. Equimolar amount of oxalate and metal does not result in complete precipitation and around 50% excess of oxalate is required. Yields of oxalates can be enhanced by precipitating in presence of alcohols as they reduce the solubility product of the oxalate in the solution. This method has been widely used for preparation of rare earth oxalates (Konishi *et al.*, 1998; Iglesias *et al.*, 1999; Ropp *et al.*, 1969.)

Mixtures of oxalic acid with ammonium oxalate or sodium oxalate are also used as precipitating agents (Zielnki *et al.*, 1998). Oxalic acid with sodium oxalate allows effective recovery of metals (Wojciechowska *et al.*, 2017). However, addition of ammonium oxalate to the oxalic acid solution does not improve its stripping and precipitating properties. Potassium oxalate solution itself has a low precipitating capacity. Addition of oxalic acid to the same increases H^+ ion availability and the precipitation (Campbell, 1999). Carbon dioxide and water as a stripping agent in PS for preparation of La and Y rare earth carbonate powders are also reported (Konishi and Noda, 2001). Table 6.1 gives the details of oxalates prepared using the PS technique. The effect of parametric variations on the particle formation, morphology and the PSD are also detailed.

Precipitation-stripping is also used for preparing fine particles in the internal droplets of W/O emulsions in an Emulsion Liquid Membrane (ELM) system (Sengupta *et al.*, 2011; Hirai *et al.*, 1996, 1999; Qiu *et al.*, 1999). The reaction leading to oxalate formation takes place in the aqueous internal droplets of an ELM that are of restricted size hence, the size and morphology of the particles can also be controlled (Hirai *et al.*, 1999). Submicron sized particles of nickel oxalate (Sengupta *et al.*, 2011) copper oxalate (Hirai *et al.*, 1996) as well as oxalates of Ce, Pr, Nd and Gd La, Dy and Y have been prepared in ELM systems (Hirai *et al.*, 1998).

The major difference between an ELM system and PS system stems from the fact that in an ELM system the particles get synthesized in the confined space of stripping phase droplets (3 to 10 μm) which are largely stagnant within the emulsion globules of size 0.5 -3mm. The maximum particle size is restricted to the internal droplet size of the W/O emulsion.

Table 6.1 Oxalates prepared using PS technique and effect of parametric variations

Metal	Extractant	Stripping agent	Remarks on stripping/ parametric effects	Reference
Yttrium	0.5M D2EHPA	0.5-0.75M Oxalic acid in HNO ₃	<ul style="list-style-type: none"> • Increase in oxalic acid concentration enhances stripping rate and also results in a higher yield. • Increasing the acidity (HNO₃ conc.) of the oxalic acid solution results in faster kinetics. 	Iglesias <i>et al.</i> , 1999
	0.8-2.2M HDHP	0-5 M nitric acid, 0.15-0.75M oxalic acid	<ul style="list-style-type: none"> • Increase in oxalic acid concentration increases precipitation yield and solubility of yttrium in the aqueous phase decreases 	Combes <i>et al.</i> , 1997
	0.99 to 1.99 M Versatic 10	0.92 -1.78M oxalic acid	<ul style="list-style-type: none"> • Increase in stirring speed (100-1000rpm) decreases the particle size. • Longer mixing time (0.5-5 Min) appears to produce finer particles • Particle size decreases as oxalic acid concentration decreases. 	Konishi <i>et al.</i> , 1998
	0.97 M Versatic acid	0.049 M oxalic acid	<ul style="list-style-type: none"> • Addition of HCl to oxalic acid results in an increase in particle size 	Konishi <i>et al.</i> , 1993
	HDEHP	0.15 to 0.8M oxalic acid	<ul style="list-style-type: none"> • Stripping rater increase with oxalic acid concentration and with temperature. • Stripping rate decreases as extractant concentration increases. 	Combes <i>et al.</i> , 1997
Yttrium and Lanthanum	0.23M MEHEHP	1M oxalic acid	<ul style="list-style-type: none"> • 80.1% Yttrium and 90.3% Lanthanum precipitate 	Smith, 2007
	0.104M Versatic 10	Carbon dioxide gas and distilled water	<ul style="list-style-type: none"> • T= 10-80 °C , P= 0.1-3.0 MPa., t=2hr , stripped as lanthanum carbonate, Yttrium carbonate. 	Konishi and Noda, 2001
Yttrium, Barium, Copper	-----	Water + oxalic acid Ethanol + oxalic acid Propanol + oxalic acid	<ul style="list-style-type: none"> • Precipitation in ice bath at 0-2 °C with propanol oxalic acid system yield metal oxalates with a minimal loss 	Shter and Grader, 1994

Lanthanum and Neodymium	40 Wt% Rokanol PIO	Potassium sulfate, sodium sulfate or ammonium sulfate to sulphuric acid solution.	• Studied the effect of strippant composition on rate of stripping	Zielinski <i>et al.</i> , 1991
Lanthanide	D2EHPA	15 wt% H ₂ SO ₄ and 20 wt% H ₂ SO ₄ with 5, 10 and 15 wt% of Na ₂ SO ₄	• Studied the effect of strippant composition on rate of stripping	Zielinski <i>et al.</i> , 1993
Bismuth	1.44M - 3.60MTBP	20% oxalic acid	• phase ratio (O:A) 1:1 suitable for stripping	Wang <i>et al.</i> , 2016
Copper	30% (v/v) N902	0.02 to 0.012 M ,Oxalic acid	• Size of ultrafine copper oxide powders was not impacted when the oxalic acid conc. decreased from 0.02 to 0.012M	Zhu <i>et al.</i> , 2013
Indium	Cyphos® IL 101 Aliquat® 336	Milli-Qwater, ethylenedi aminetetraacetic acid disodium salt dehydrate, NaOH	• Stripping temp;60 ⁰ C Indium recovered as In(OH) ₃ by stripping with a NaOH	Deferm <i>et al.</i> , 2016
Zinc	TBP	0.1-0.5M oxalic acid	• particle obtained in 0.1 M and 0.5M of oxalic acid were very irregular and flat but their size was slightly decreased at 0.5M oxalic acid conc.	Lee <i>et al.</i> , 2017
	HDEHP	oxalic acid ethanol aqueous solution	• 0.3 Moxalic acid in 80% v/v ethanol solution yield 36nm size zinc oxalate	Zhang <i>et al.</i> , 2008
Zinc and Iron	Cyanex 923 (0.25–1.76 M)	0.5 M to 2 M Oxalic acid	• Increase in oxalic acid concentration stripping of both Fe and Zn increased • Fe is also stripped with oxalic acid, but it would remain in the soluble form.	Sinha <i>et al.</i> , 2016
Zinc, Lead, Copper, Cadmium, Nickel	30% D2EHPA	Oxalic acid (with and without ammonium oxalate)	• By using ammonium oxlate as additive the stripping and precipitation yields were decreased and not more than 83% of metals could be recovered as precipitate	Zielinski <i>et al.</i> , 1998
Samarium	VA10 D2EHPA	Oxalic acid	• Oxalic acid 1-2M	Sanuki, 1994

This result in a narrow size distribution of the particles obtained. In PS systems there is no such space confinement and the stripping phase is in an agitated state (Sengupta *et al.*, 2011).

6.2 Experimental

The brass rinse liquors contained copper and zinc and traces of other elements as shown in Table 6.2. Experimental methodology adopted for extraction and stripping was identical to that used to recover the metals from Brass pickle liquor detailed in Chapter 4. The design of the circuit was also identical.

Extraction

Copper was extracted using 10 % (v/v) LIX 84-IC in kerosene at equal volume of organic to aqueous phase. Zinc was extracted using 10% (v/v) D2EHPA. The pH of the aqueous phase after copper extraction was 2.5, which was in the pH range for zinc extraction using D2EHPA thus requiring very little pH adjustment.

Table 6.2: Composition of brass rinse liquor

Component	Concentration (g/L)
Cu	4.387
Zn	2.780
Na	1.72
Mg	0.184
Ni	0.097
Ca	0.060
Al	0.036
Fe	0.031
Mo	0.0077
Sn	0.0004
Chlorides	2.74
pH	1

Precipitation- Stripping

Precipitation-Stripping was carried out as discussed in Chapter 4. The parameter space of PS was thoroughly explored for both copper precipitation and zinc precipitation. The effects of oxalic acid concentration, shaking speed and contact time between organic phase and the aqueous oxalic acid as well as metal loading on the yield, morphology and the particle size distribution of the oxalate particles was determined.

Particle characterization

The precipitated copper and zinc oxalates and their respective oxides were characterized using XRD, FTIR, EDX, and their PSD were determined by laser diffraction techniques, their morphology studied by FESEM as per standard operating procedures discussed in Chapter 3. Antibacterial properties of the copper and zinc oxides were also evaluated; the details are discussed in Section 6.5.

6.3 Results and Discussion

6.3.1 Extraction

Speciation diagram generated on the basis of copper, zinc and chloride concentrations shown in Figure 6.2 that copper and zinc both exist as the bivalent specie. In view of the copper and zinc concentration in the rinse liquors the organic phase for copper extraction was prepared with 10% of LIX 84-IC while the organic phase for zinc extraction contained 10% D2EHPA. Single stage extraction was sufficient to extract 4.365 g/L copper accounting for 99.5% extraction at an equilibrium pH of 2.5 similarly 2.747 g/L zinc was extracted accounting for 98.8% zinc at an equilibrium pH of 3

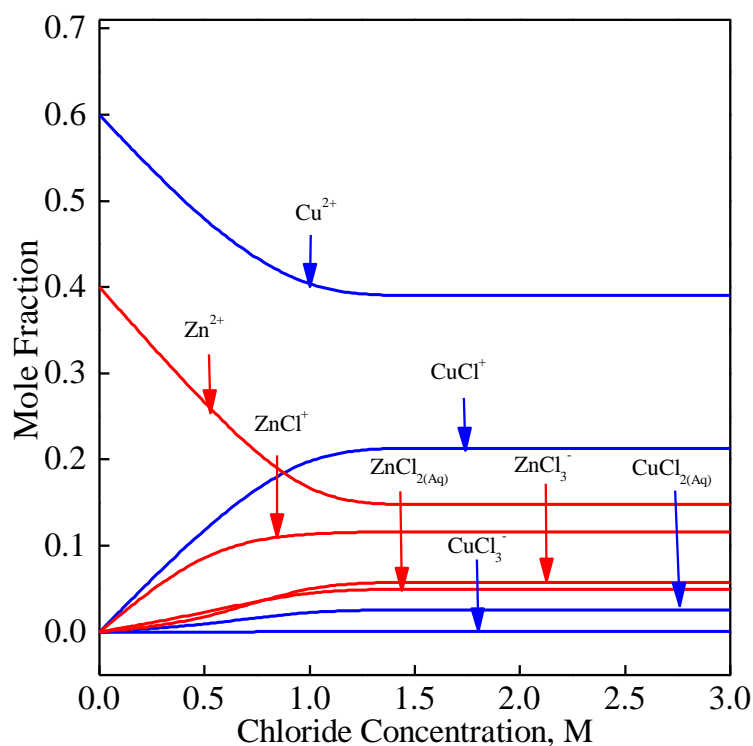


Fig. 6.2: Speciation diagram of copper and zinc in brass rinse liquor as a function of chloride concentration

The mechanism of extraction of copper using LIX is considerably different from zinc using D2EHPA in view of LIX being a chelating extractant which binds the metal by clawing (holding at two sites) while D2EHPA is an acidic extractant which has characteristic that sometimes resemble chelating extractants and sometimes is similar to solvating extractants. Hence, the stripping behaviors are also expected to be different.

6.3.2 Effect of agitation speed and time on the Precipitation-Stripping of copper and zinc

It is reported in the literature that LIX is insoluble in water therefore stripping will take place of at the oil water interface (MCT Red book 1998), whereas, D2EHPA exhibits phase transfer behavior hence, stripping is likely to take place in the aqueous phase (Huang and Juang, 1986). Necessarily, stripping would be more rapid in D2EHPA systems in comparison to LIX systems. In view of the fundamental difference in the mechanisms of stripping it is easy to foresee that intensity of agitation that leads to creation of phase boundaries and also leads to the shrinkage of boundary layer thickness / film thickness of both organic and aqueous phase which has an accelerating effect on the rates of stripping.

Therefore, a major parameter that is expected to influence the stripping patterns, particle size and the size distribution of the particles is the rate of agitation. However, size of the particles and the size distribution will also be sensitive to other processing parameters viz. stripping time, metal loading in the organic phase and the concentration of the stripping agent.

PS experiments were also carried out at shaking speeds of 50, 100 and 150 rpm using 1M oxalic acid solutions for varying time intervals. Contact between the organic phase and aqueous oxalic acid was performed in shake flasks that are essentially not dispersive as in regular agitation systems involving two heterogeneous phases. At low shaker speeds (rpm) the phases rub with one another at the interface but at higher speeds, phases show tendency of breaking down and big chunks of liquid move in to the other phase as in intermingling of phases. This intermingling of phase's increases with shaking speed and the fluid chunks become smaller in size. The consistency of agitation in shaker is very high.

Effect of three shaker speeds were investigated and the yield of particles (metal values) at the end of a run was taken as a measure of the amount stripped since, amount of oxalate soluble in oxalic acid solution was extremely low. Figure 6.3a represents the kinetics of stripping of copper at three different stripping speeds. Each data point in the plot represents

an individual experiment. Therefore, passing of curves from such discrete data points truly reflects on the real nature of stripping kinetics.

Effect of shaking speed is quite pronounced in case of copper stripping. There is 15% to 20% increase in yield by increasing the shaking speeds from 50 rpm to 100 rpm and then to 150 rpm. A plateau in the yields was observed only at 150 rpm and that too at 240 min. Contrary to copper stripping behavior, the stripping pattern for zinc (Figure 6.3b) is much more rapid.

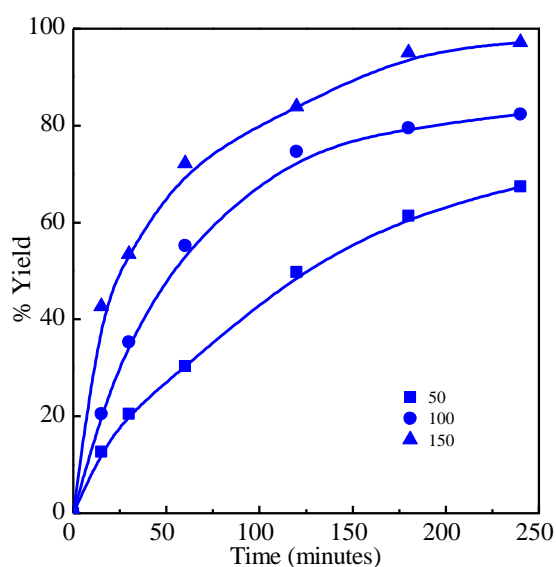


Fig.6.3a:Effect of RPM on copper stripping (Cu- 4.365 g/L, oxalic acid 1M)

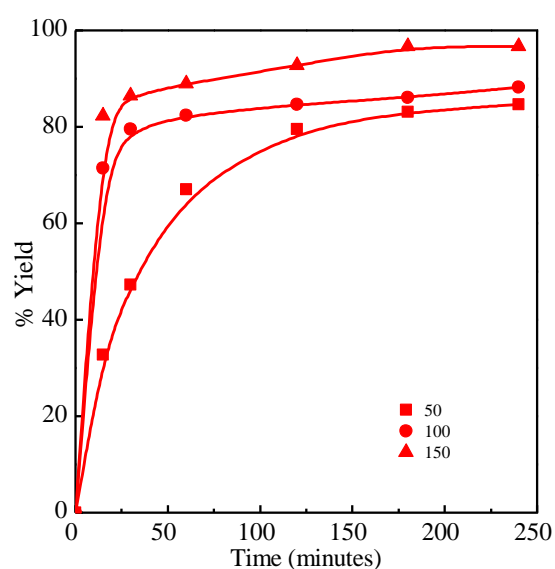


Fig. 6.3b: Effect of RPM on zinc stripping (Zn- 2.73 g/L, oxalic acid 1M)

Effect of rpm is visible but much less pronounced. The final yields are just 10% apart at 240 min. when rpm is increased from 50 rpm to 150 rpm. Plateau in yields are reached in 120 min time at shaking speeds of 100 rpm and 150 rpm. At speeds of 50 rpm the plateau is reached at 180 minutes.

It can be clearly made out from Figure 6.3b that zinc strips faster than copper, the reason attributed to this difference in stripping rates is primarily due to the differences in the binding of the metal ions with the extractant. The chelating extractant LIX 84-IC holds copper ion by clawing at two points resulting in stronger binding in comparison with the solvation of zinc ions by D2EHPA. Further, LIX 84-IC is immiscible in water therefore stripping has to occur at the interface between oil and water. In non-dispersive agitation the interface is limited, slowing down the stripping rates. As the shaking rates increase there is an increase

in the interfacial area because increased momentum of fluids lead to an element of dispersion of water in oil phase by virtue of convection rolls. This phenomenon is more pronounced at still higher shaking rates. Thus, enhanced rates of shaking not only keep each of the phases well mixed but also increases the interface and squeezes the boundary layer in both the phases resulting in an increase in the stripping rates.

On the other hand, for the case of stripping of zinc, since the extractant D2EHPA has partial miscibility in water, due to phase transfer effect, D2EHPA transfers along with solvated zinc into the aqueous boundary layer to encounter a much larger amount of H^+ ions than at the interface and gets stripped of zinc more rapidly while the extractant phase transfers back to the oil phase. In this case not only stripping but precipitation is also expected to be more rapid due to the excess of oxalate ions in the aqueous phase. For the stripping of zinc, an increase in interfacial area due to an increase in shaking speed will be much more pronounced than that for copper at early stages of stripping since stripping is faster as observed in Figure 6.3b.

Size distribution of copper oxalate particles

The size distribution obtained for copper oxalate particles at different time intervals after 15 min, 1 hr and 3 hr of precipitation time at three shaking speeds is shown in Fig 6.4a, b and c respectively. In addition to this the particle size distribution obtained at 150 rpm shaking speed after stripping times of 15min, 1 hr and 3 hr are compiled in Figure 6.4d.

It is seen in Fig 6.4a that at 50 rpm the particles obtained vary from 100 nm to 60 μm in size. The median in distribution is at $\sim 3 \mu\text{m}$, the overall distribution is Gaussian, there is a fair amount of small particles up to 300 nm and on the other side of the spectrum there are number of particles greater than 30 μm .

At 100 rpm, the particles display a narrower distribution with the smallest particles being 400 nm and the largest going up to 100 μm . There appears to be some hindrance of the particles growing from 400 nm to 1000 nm thereafter, the growth is rapid. Similarly, above 20 μm particle size there are quite a number of particles hinting at agglomeration of particles. At 150 rpm shaking speed and 15 min precipitation time particles ranging from 300 nm to 30 μm size are obtained. The picture emerging indicates bimodal distribution with $\sim 20 \mu\text{m}$ agglomerates.

After 1 hr duration the particles seem to have grown considerably and there is a shift of distribution to larger sizes. Even at 50 rpm shaking speeds the smallest particles were of 300nm size and there was a concentration of small sub-micron sized particles in this distribution but, the distribution was narrower than that observed at 15 min time. At 100 rpm the nature was almost the same as found in 15 min but a narrow distribution was there. The number of large sized particles was low and the distribution ended at 20 μm at 150 rpm shaking speed again a bimodal type distribution is observed. The nature of the curve indicates there are considerable amount of submicron particles awaiting growth.

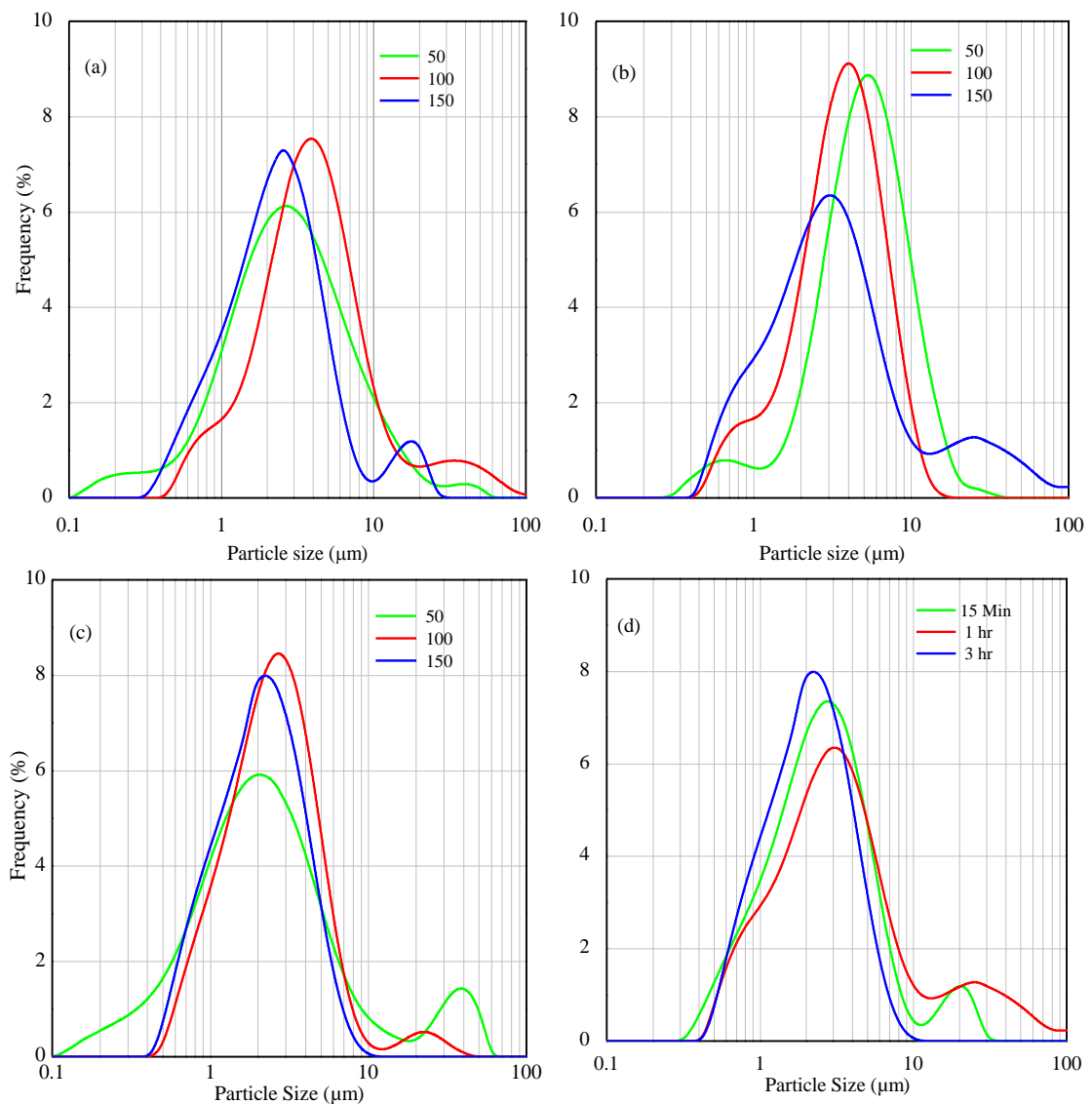


Fig. 6.4: PSD of copper oxalate: Effect of RPM

(a) 15 min (b) 1hr (c) 3 hr, (d) 150 rpm

Copper oxalate particles collected after 3 hr of precipitation time shows a PSD similar to that observed after 15 min and 1 hr but some significant differences are also observed in Figure 6.4c. At 50 rpm shaking speeds again a very wide size distribution ranging from 100 nm to 70 μm is seen. The distribution is bimodal indicating agglomeration of particles that leads to median particle size of 40 μm . The size distribution of particles at 100 rpm and 150 rpm speeds have narrow distribution, there is tendency of bimodal distribution at 100 rpm. The narrowest distribution is observed at 150 rpm ranging from 0.4 μm to 10 μm .

Figure 6.4d shows the distribution obtained at 150 rpm as a function of time and brings out some salient aspects. With increasing time, the distribution becomes narrower, bimodal tendency is prevalent at low time scales. The disappearance of bimodal pattern is attributed to breakage of agglomerates under prolonged influence of shear. The PSD shows a marginal shift towards smaller size range with time. Particularly at 1 hr time span there is quite a number of smaller submicron particles that deflects the distribution from Gaussian. The particle size distributions show that there are many processes going together at the same time, nucleation, growth of nuclei, growth by aggregation and some secondary nucleation. The statistical distribution at varying shaking speeds and time intervals for copper oxalate particles are shown in Table 6.3.

Table 6.3: Statistical distribution of copper oxalate particles: Effect of RPM and time

RPM	Time	D [3 2]	D[4 3]	D[0.1]	D[0.5]	D[0.9]
50 rpm	15min	1.400	3.62	0.69	1.87	9.65
	1h	3.060	2.88	0.25	2.21	6.37
	3h	1.880	4.2	1.46	3.78	7.45
100rpm	15min	2.600	6.4	1.24	3.59	10.95
	1h	2.437	3.76	1.22	3.37	6.77
	3h	1.86	6.43	0.84	2.51	7.02
150 rpm	15min	1.7	3.4	0.79	2.32	5.98
	1h	2.1	8.24	0.9	2.9	21.7
	3h	1.59	2.43	0.78	2.05	4.6

Size distribution of zinc oxalate particles

Zinc strips faster than copper for the reasons discussed earlier, this aspect influences the PSD. Particles obtained at 15 min ((Figure 6.5a) show the same width of distribution for both 100 rpm and 150 rpm but at 100 rpm particles are in general smaller in size. 50% particles ($d_{0.5}$) are smaller than 3.15 μm , while at 150 rpm they are 10 μm in size. There is a predominance of small size particles in the PSD present which could grow with passage of

time and alter the distribution. Particles obtained after 1 hr (Figure 6.5b) time span at 150 rpm shows Gaussian distribution. At this time 50% of the particles are less than 3.49 μm . The distribution obtained at 100 rpm and 1hr is also Gaussian. At 50 rpm and 1 hr a very wide distribution was obtained.

The distributions observed for 3 hrs ((Figure 6.5c) duration were relatively narrow at 150 rpm but the distribution showed broadening for 100 rpm and 50 rpm. There appears to be aggregation of particles in the larger size range at lower rpm's that are not seen at 150 rpm.

It gives credence to the idea that at lower rpm's instable aggregates get formed that break down at higher shears at 150 rpm.

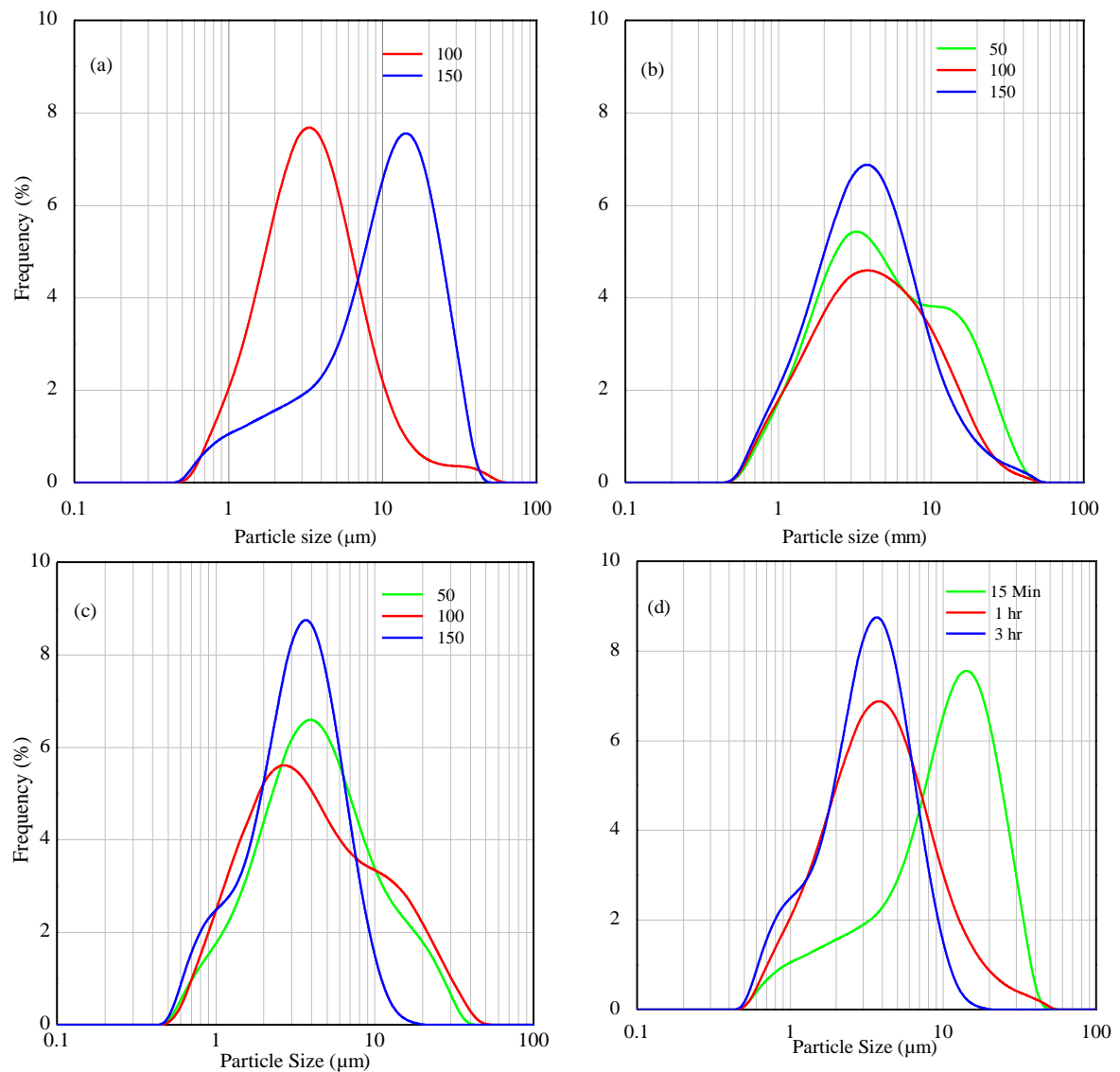


Fig.6.5: PSD of zinc oxalate: Effect of RPM (a) 15 Min (b) 1hr (c) 3 hr (d) 150 RPM

Effect of time on particle size distribution of zinc oxalate at 150 rpm shaking speed is shown in Figure 6.5d. At 15 min a very sizeable number of small particles along with aggregates of larger sizes - a skewed distribution is observed.

Table 6.4: Statistical distribution of zinc oxalate particles: Effect of RPM and time

RPM	Time	D [3 2]	D[4 3]	D[0.1]	D[0.5]	D[0.9]
50	1h	3.02	3.06	1.34	4.27	17.15
	3h	2.8	5.68	1.3	3.87	12.88
100	15min	3.1	2.6	1.26	3.15	8.27
	1h	2.84	2.43	1.23	3.36	10.21
	3h	2.59	1.86	1.16	3.48	15.13
150	15min	4.81	1.7	1.93	10	22.4
	1h	2.6	2.1	1.23	3.49	10.6
	3h	2.23	1.59	1.034	3.07	6.84

At 100 rpm the picture changes and a Gaussian distribution is observed, while at 150 rpm there is an increase in sub-micron particles that could have formed at late stages of precipitation due to high churning of oil phase at 150 rpm. If one looks closely at the zinc oxalate precipitate yield plots, Figure 6.3b at 150 rpm the maxima in precipitate yields is attained at 180 minutes thereafter there is plateau in yield. The statistical distribution of particles is listed in Table 6.4 makes it apparent that with increase in shaking speed narrow size distributions are obtained.

6.3.3 Effect of oxalic acid concentration on the Precipitation-Stripping of copper and zinc

The influence of oxalic acid concentration on the precipitation stripping of copper oxalate and zinc oxalate was explored over oxalic acid concentrations (Figure 6.6) ranging from 0.078 M to 1M for copper oxalate and 0.057M to 1M for zinc oxalate stripping at 150 rpm shaking speeds and a time duration of three hours.

The lowest concentrations of the oxalic acid in both the cases correspond to condition of equal moles of copper to acid and zinc to acid in the system. Copper loading in the system was 4.365 gm/lit and that of Zn was 2.747 gm/L.

Precipitation of copper increases with acid concentration and reaches plateau at 0.5 M acid concentration further increasing acid concentration to 1.0 M increases the precipitate yield

by just 2 %. The data fits a smooth curve as seen in Figure 6.6. Zinc precipitation on the other hand is jerky, at lower acid concentrations more amount of zinc is precipitated in comparison with copper but the yield of precipitates at 0.5 M and 1.0 M acid concentration differs by only about 5%.

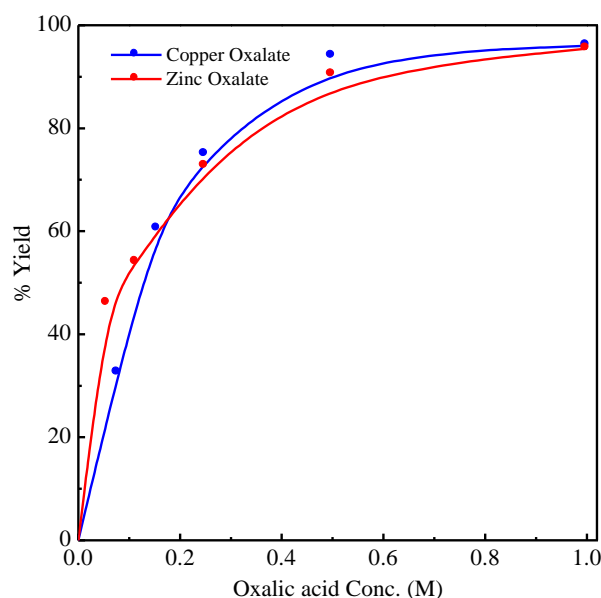


Fig. 6.6: Effect of oxalic acid concentration on yield of copper oxalate and zinc oxalate

The yield of precipitates of copper and zinc are shown in Figure 6.6 and the experimental and predicted yields of metal stripped are given in Table 6.5 and Table 6.6 for copper and zinc oxalate respectively.

Table 6.5: Effect of oxalic acid concentration on copper recovery

Oxalic acid Conc. (M)	Copper loaded 4.365 g/L						% Yield	
	Amount(gm)				E			
	Experimental		S	Predicted				
	P	Sl		P	Sl			
0.078	1.42	0.01	1.43	1.4231	0.0069	32.53	32.60	
0.156	2.642	0.028	2.67	2.662	0.008	60.52	60.98	
0.25	3.271	0.039	3.31	3.301	0.009	74.93	75.62	
0.5	4.105	0.045	4.15	4.137	0.013	94.04	94.77	
1	4.192	0.048	4.24	4.222	0.018	96.04	96.72	

S: Stripped, P: Precipitated, E: Experimental, T: Theoretical, Sl: soluble

The precipitation data (Table 6.5 and Table 6.6) reflects the fast stripping tendency of zinc at 0.057M condition. Zinc oxalate precipitation is 46% while copper oxalate precipitation is 32.5%. However, increasing acid concentration to 0.25 M, copper oxalate yield is ~ 75% while zinc oxalate yield is 72.6% although molar ratio of metal to acid is more for zinc than copper. These results indicate that while copper precipitation is very sensitive to acid concentration zinc is not so perhaps due to differences of mechanism governing stripping from the extractants.

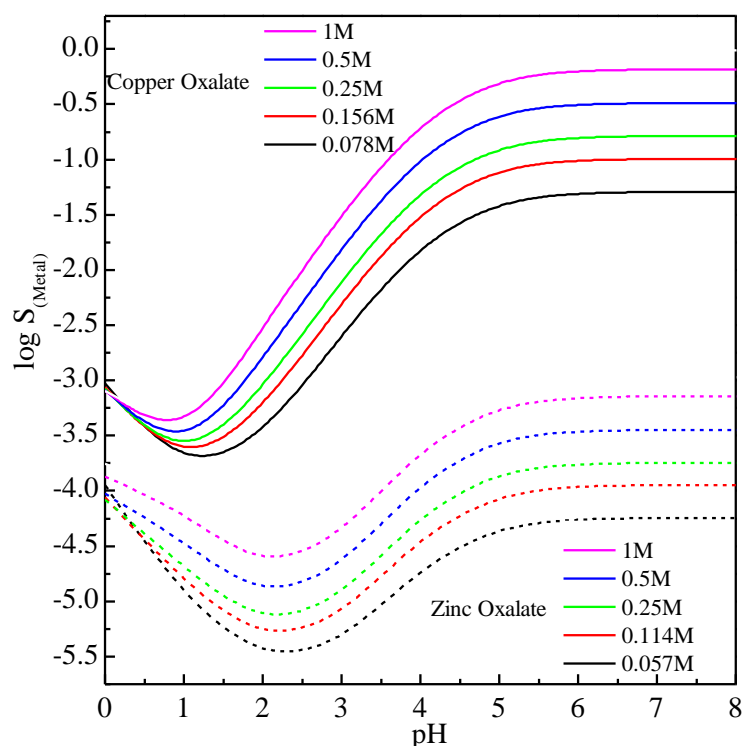


Fig.6.7: Solubility curves of copper oxalate and zinc oxalate at varying oxalic acid concentrations

The amount of oxalate remaining dissolved in the stripping solution was determined experimentally and also predicted based on theoretical considerations. The required solubility diagram (Figure 6.7) at varying oxalic concentrations for both copper and zinc was developed using the method detailed in Chapter 4.

The PSD of the precipitates (Figure 6.8) obtained is fairly narrow for copper oxalate ranging from 400 nm to 50 μm , particles obtained at acid concentration of 0.078 M is well defined. Increasing the acid strength to 0.156 M shows agglomeration in particles formed as well as possibility of delayed precipitation of particles.

Table 6.6: Effect of oxalic acid concentration on zinc recovery

Oxalic acid Conc. (M)	Zinc loaded 2.747 g/L						% Yield	
	Amount(gm)					E		
	Experimental		S	Predicted				
	P	Sl		P	Sl			
0.057	1.278	0.0016	1.28	1.28	0.0004	46.085	46.13	
0.114	1.497	0.0028	1.5	1.49	0.0006	53.97	54.05	
0.25	2.016	0.0039	2.02	2.019	0.0009	72.67	72.78	
0.5	2.509	0.0046	2.514	2.50	0.006	90.46	90.41	
1	2.648	0.0068	2.655	2.65	0.0012	95.46	95.66	

S: Stripped, P: Precipitated, E: Experimental, T: Theoretical, Sl: soluble

Delayed precipitation seems more pronounced in precipitates formed by reacting with 0.5 M acid strengths and is also observed in particles formed with 1.0 M acid strengths. Tendency towards bimodal distribution is also seen in copper oxalate precipitates in the latter case.

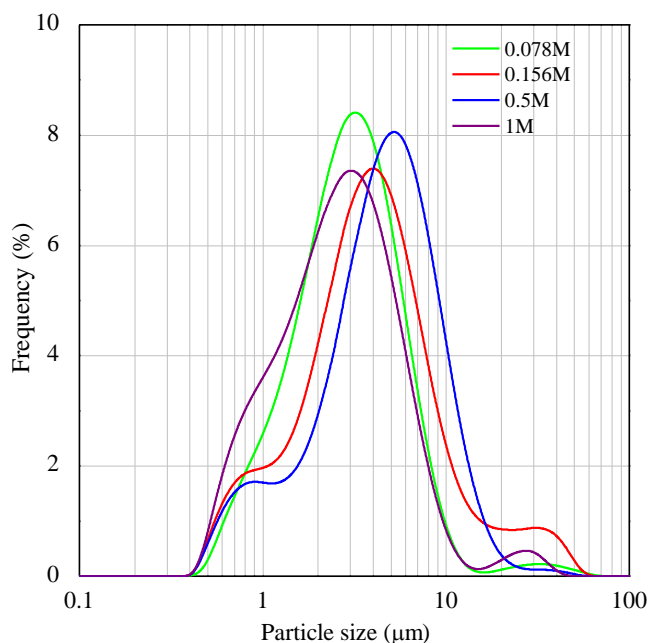


Fig. 6.8: Effect of oxalic acid concentration on copper oxalate (Cu= 4.365 g/L, t=3 hr)

Zinc oxalate formed by PS shows a movement towards smaller particle sizes with an increase in the oxalic acid concentration (Figure 6.9). Stripping with 0.057 M acid shows well defined and narrow particle size distribution having ~20 µm average size, however, smaller size particles are also present separate from the main distribution. Increasing the acid

concentration to 0.114 M again has the average size of the particles $\sim 20 \mu\text{m}$ but widens the distribution, there is a large number of smaller particles that either may have been formed at late stages of precipitation or numerous particles that could not grow. Precipitates formed by 0.5 M acid produces a very broad distribution with small particles showing tendency to grow, while particles generated with contact with 1.0 M acid produces a relatively narrow size distribution with an average size of $3 \mu\text{m}$.

The PSD plots obtained for copper oxalate and zinc oxalate precipitation by oxalic acids of varying concentration reveal the influence of acid strength on stripping. In the case of copper

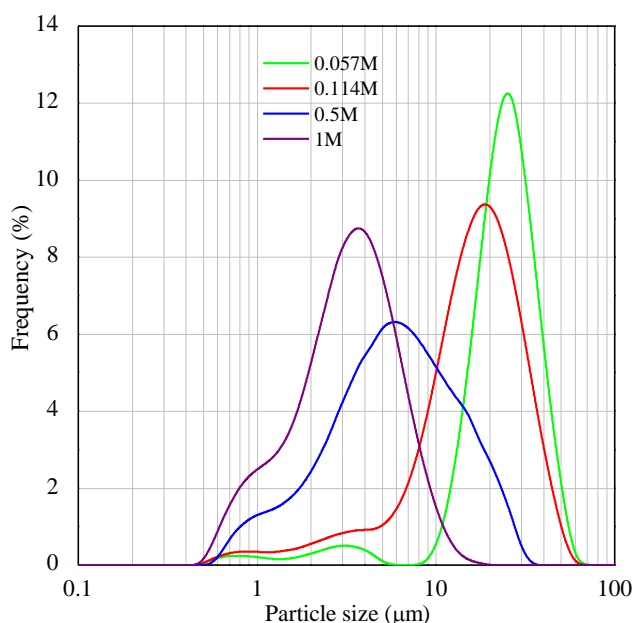


Fig.6.9: Effect of oxalic acid concentration on zinc oxalate (Zn= 2.73 g/L, t=3 hr)

the effect of acid strength is visible but doesn't alter the distribution substantially. At higher acid concentrations one can observe the effect of late precipitation of oxalates affecting the distribution.

Table 6.7: Statistical distribution of copper oxalate particles: Effect of oxalic acid concentration

Oxalic Acid Concentration	D [3 2]	D[4 3]	D[0.1]	D[0.5]	D[0.9]
0.078 M	2.115	3.537	1.06	2.73	5.97
0.156 M	2.412	5.497	1.052	3.545	10.446
0.5 M	2.678	5.024	1.1	4.23	9.39
1 M	1.590	2.87	0.75	2.07	5.33

The PSD obtained for zinc oxalate shows drastic effect of acid strength on stripping. At very

low acid strength, limited number of particles get formed that grow with time yielding large average sizes. As acid strength increases the distribution shifts towards smaller sizes which could be due to formation of large number of nuclei in the system.

Table 6.8: Statistical distribution of zinc oxalate particles: Effect of oxalic acid concentration

Oxalic Acid Concentration	D [3 2]	D[4 3]	D[0.1]	D[0.5]	D[0.9]
0.057 M	9.39	19.49	8.78	18.26	32.73
0.114 M	8.9	19.46	8.89	18.3	32.6
0.5 M	4.2	5.54	2.75	4.87	8.78
1 M	2.232	3.62	1.034	3.07	6.84

6.3.4 Effect of metal loading on the Precipitation-Stripping of copper and zinc

Organic phase loaded with different amount of the metal values were stripped using 1 M oxalic acid for a period of 3 hours at 150 rpm shaking speed. Figure 6.10a, shows the PSD for copper oxalate obtained from an organic phase loaded with 4.365 g/L copper resulting in a copper yield of ~96% in single stage recovery and the second PSD is for an oil phase loaded with 13.17 g/L copper that on treatment with oxalic acid resulted in single stage yield of 66.66%. Comparing the two PSD one finds that in spite of very different amount of particles precipitated in both cases the PSD's are very similar, even the width of the distribution is nearly same, except that in the PSD with higher copper content in oil phase there is a plausibility of delayed precipitation.

Zinc oxalate precipitation from oil phases, loaded with 9.72 g /L and 2.74 g/L of zinc, at 150 rpm shaking speeds for 3 hr at equal oil to aqueous phase volumes resulted in precipitate yield of 78.5% and 95.46% respectively for single stage contact. Necessarily much larger amount of precipitates was formed when the oil phase containing more zinc was stripped.

However, no significant difference between the PSD's are observed, both the distributions are fairly narrow and well-formed particularly in the post median part (Figure 6.10b). There is greater amount of fine particles in the PSD of precipitates from oil phase with 9.72 g/lit of zinc that could be due to delayed precipitation or breakup of small aggregates due to shear. In general, it could be concluded that metal loading in the oil phase does not have a significant influence on particle size distribution.

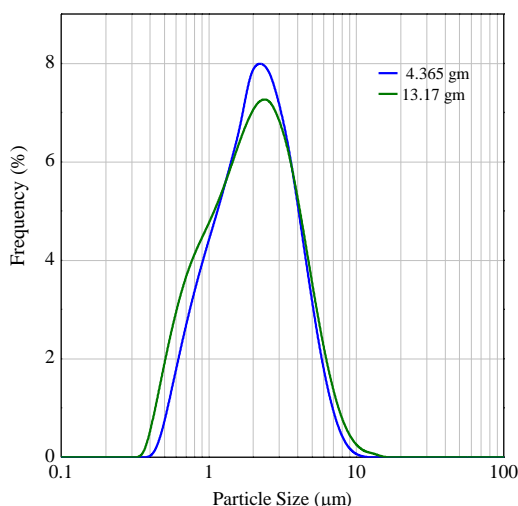


Fig.6.10a: PSD of copper oxalate: effect of metal loading (t=3 hr, oxalic acid =1M)

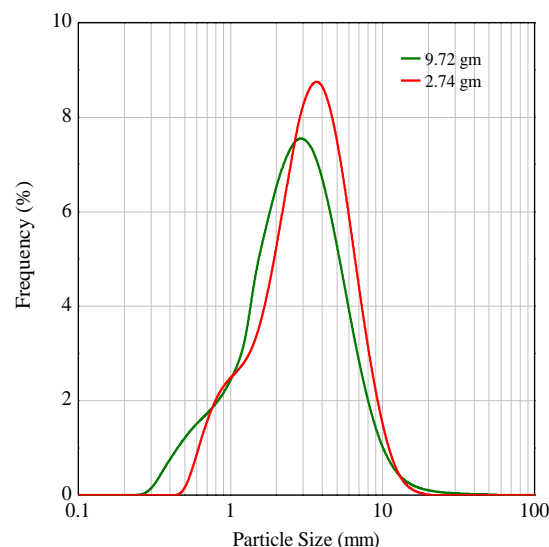


Fig. 6.10b: PSD of zinc oxalate: effect of metal loading (t=3 hr, oxalic acid =1M)

6.3.5 Characterization of oxalates and oxides

The precipitated oxalates and their respective oxides were characterized using XRD, IR and EDX as discussed in Chapter 3. The XRD patterns of copper and zinc oxalate and their respective oxides are shown in Figure 6.11. The diffraction data for copper oxalate matched with JCPDS 22-297 with crystallite size calculated by Debye Scherrer equation as 51.08 nm and or zinc oxalate matched with JCPDS 25-1029 with crystallite size of 46.8 nm. The IR spectra Figure 6.12 of the oxalates were identical to that observed in Figure 4.17 for copper and zinc oxalate.

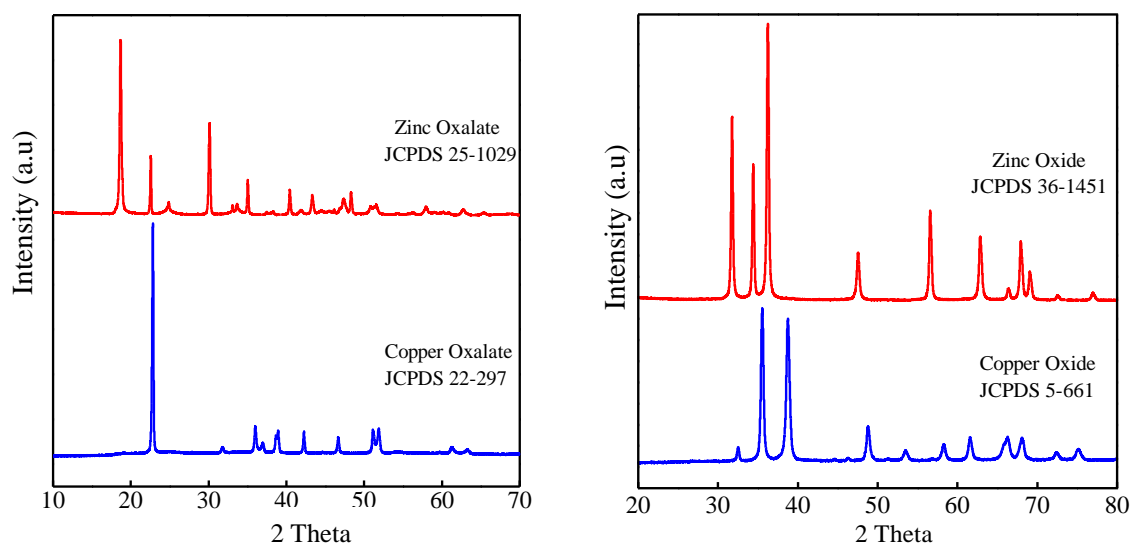


Fig. 6.11: XRD data of copper oxalate , zinc oxalate, copper oxide, zinc oxide

The copper oxalate particles were calcined at 400⁰C for 3 hours to obtain copper oxide particles while zinc oxalate was calcined at 450⁰C to obtain zinc oxide. XRD patterns revealed that pure copper and zinc oxide were formed with the diffraction data for copper oxide matching JCPDS 5-661 and for zinc oxide matching JCPDS 36-1451.

The crystallite size calculated were 53.38nm and 41.63 nm for copper and zinc oxide respectively. As expected the FTIR spectra of copper oxalate and copper oxide as well as zinc oxalate and zinc oxide (Figure 6.12) showed bands at approximately the same wave numbers as observed in Figure 4.18.

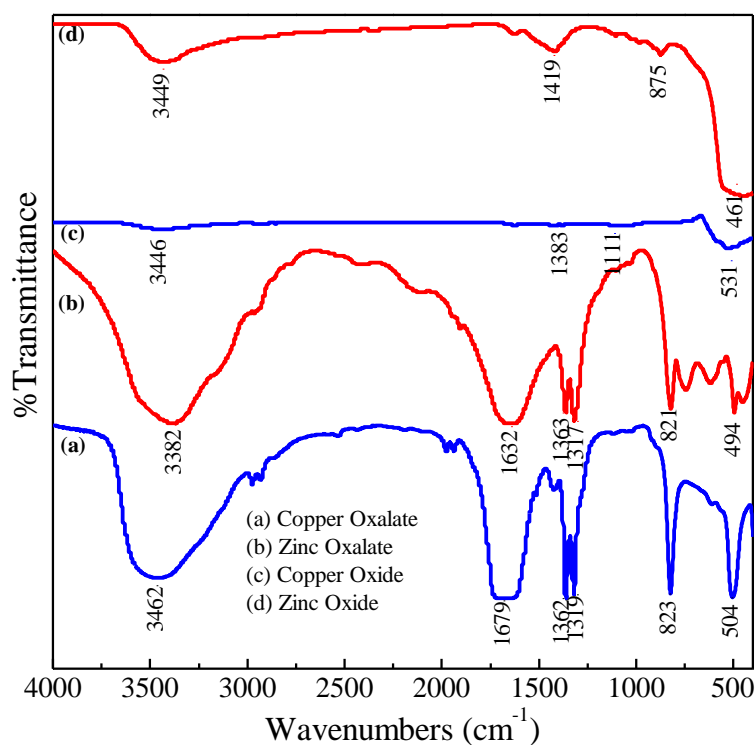


Fig. 6.12: FTIR spectra of copper oxalate , zinc oxalate, copper oxide, zinc oxide

The EDX analysis of copper oxide (Figure 6.13) and zinc oxide (Figure 6.14) confirmed pure CuO phase and ZnO phase with Cu and O and Zn and O in stoichiometric proportions. The chemical analysis of both the oxides confirmed absence of impurity indicating formation of pure copper oxide and zinc oxide.

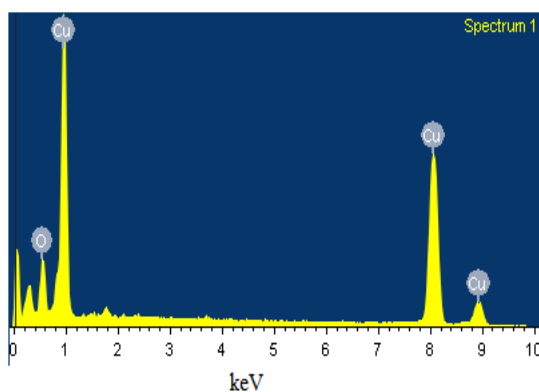


Fig. 6.13: EDX of Copper oxide

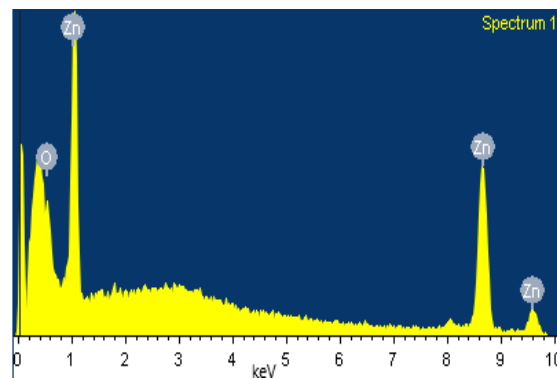


Fig. 6.14: EDX of Zinc oxide

When copper and zinc were recovered from the pickle liquor unextracted copper by LIX 84-IC was subsequently extracted by D2EHPA along with zinc and ended an impurity in zinc oxide which was detected in the EDX analysis of zinc oxide (Figure 4.21). Zinc oxide was 99.1% pure and contained 0.9% of copper oxide. However, when working with rinse waters and both copper and zinc oxide were obtained as pure products. This was due to the lower concentration of copper and zinc metals in the rinse solution that could be conveniently extracted in a single stage by the extractants. Since copper extraction was quantitative there was no copper left to move to the zinc circuit.

6.3.6 Morphology of particles formed by precipitation-stripping

Copper oxalate and copper oxide

SEM images of copper oxalate precipitated at different oxalic acid concentrations are shown in Figure 6.15. Cushion shaped morphology is observed for particles precipitated at all oxalic acid concentrations. Similar structures were observed by Soare *et al.*, 2006 when copper oxalate was precipitated using very low concentration of precursors. Figure 6.15a shows the FESEM image of the particles precipitated when the oxalic acid concentration was 0.076M accounting to a mole ratio of copper to oxalic acid of 1. Figure 6.15b which a magnified image of Figure 6a. shows two large surfaces α (hydrophobic) and four small surfaces ϵ (hydrophilic), Soare *et al.*, 2006 linked this morphology to the anisotropic nature of the crystallographic structure of copper oxalate. The α surfaces are not smooth whereas the ϵ surfaces appear to be smooth.

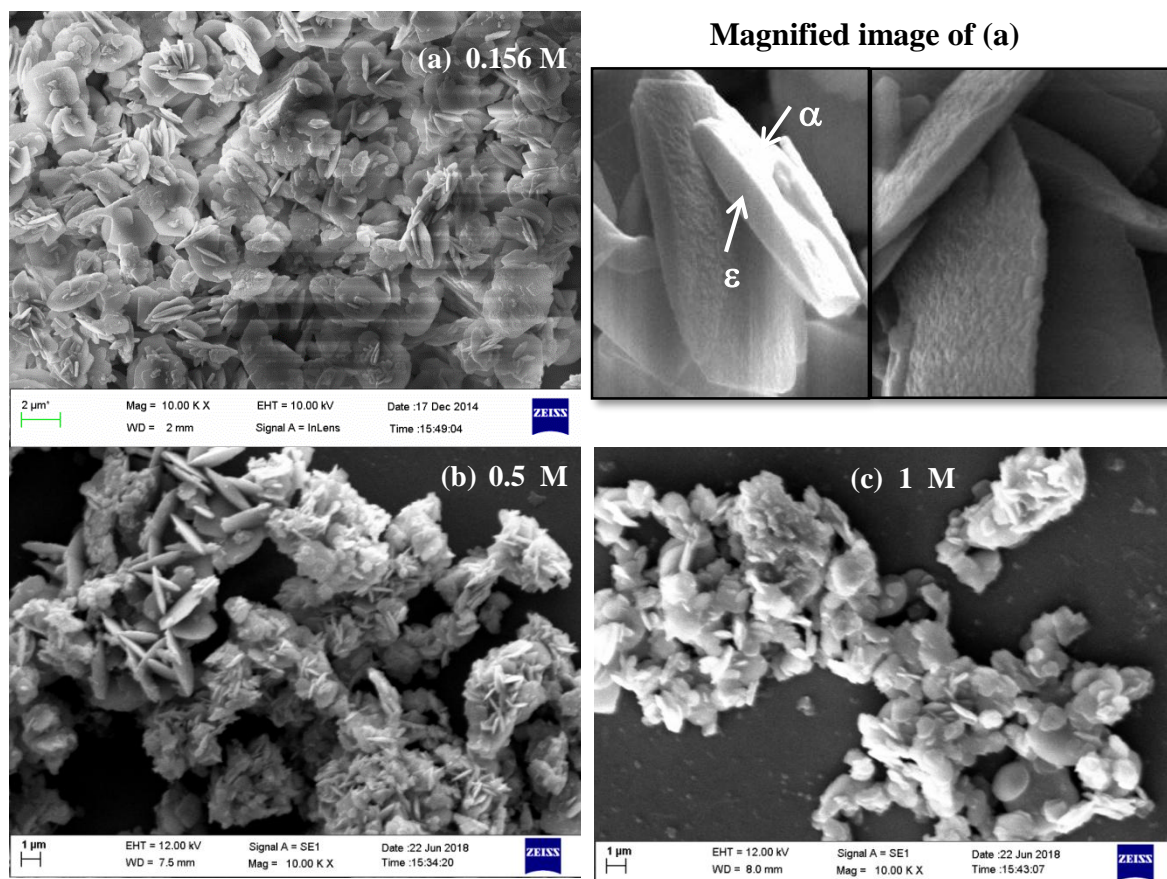


Fig. 6.15: FESEM images of copper oxalate: Effect of oxalic acid concentration (Cu=4.365 g/L, t=3hr)

In some of the particles it is observed that cushion shape has become flat at the edges. There is a dissolution of the ϵ faces both the α faces meet resulting in this morphology. Soare *et al.* (2006) observed this behavior when the particles were grown over longer precipitation times. During PS of copper the reaction takes place at the interface and copper is released slowly due to its binding by clawing mechanism with the extractant. In the time span of 3 hours of precipitation the particles which have grown by agglomeration in the initial stages become flat at the edges and those at later stages still show the bulged cushion morphology. Such cushion shaped particles have been used as anode materials for lithium ion batteries (Wan *et al.*, 2013).

The FESEM image of copper oxide obtained from the oxalate precipitated with 0.15 M oxalic acid, at 150 rpm, 3 hr duration and initial copper concentration of 4.365, g/L is shown in Figure 6.16. The FESEM of the oxalate under same conditions is shown in Figure 6.15. Comparing Figure 6.15 and Figure 6.16 it can be seen that oxalate on transformation to the oxide did not lose its ordered structure.

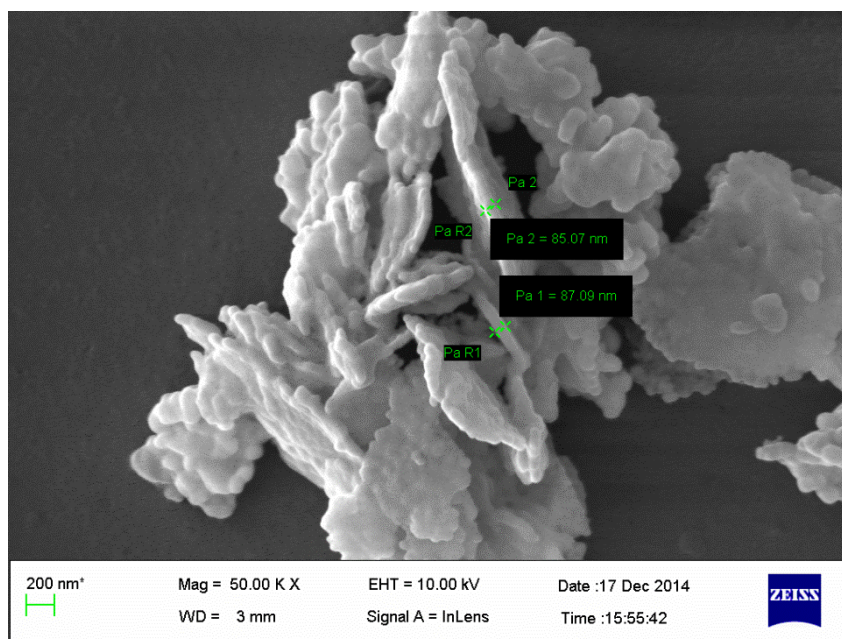


Fig. 6.16: FESEM image of copper oxide
(oxalic acid concentration=0.156M, Cu=4.365 g/L)

Zinc Oxalate and zinc oxide

Figure 6.17 shows the SEM images of zinc oxalate precipitated using 1M oxalic acid after 15 min contact time. It can be seen that some surfaces have a smooth appearance while the others are rough. This is attributed to the consolidation and cementing of all the nanocrystalline units that make up the structure resulting in the formation of smooth surface. Surfaces where this process is not complete are still rough. A layer by layer growth mechanism can be seen in the image in the inset of Figure 6.17a. SEM images also shows that the small particles are attached to the growth surfaces.

The mechanism of formation can be anticipated from the images, it can be seen that the structural boundaries are formed first and later as the nucleation proceeds, depending on their availability, nuclei are added to the framework for consolidation. During PS of zinc at 150 rpm using 1M acid concentration, more than 80 % stripping is achieved in 15 min as seen from Figure 6.3b, this results in rapid precipitation which leads to the formation of the boundaries, however, at this time not all the particles are cemented together to obtain a smooth surfaces. It is evident from Figure 6.17b inset (PSD), that there is substantial amount of smaller size particles formed during precipitation, these smaller sized particles may be the result of late precipitation it could also be due to Ostwald ripening that shifts the distribution

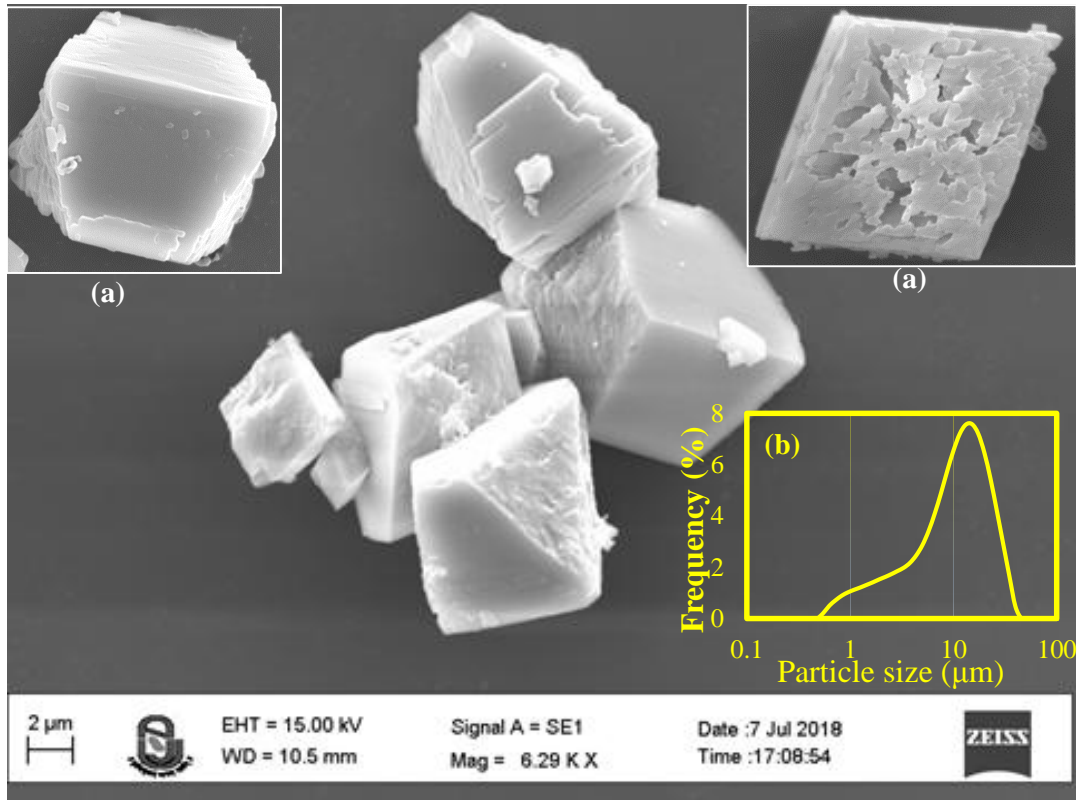


Fig. 6.17: FESEM image of zinc oxalate
(Zn=2.73 g/L, t=15 min, oxalic acid concentration=1M)

towards the dominance of larger sizes. However, it appears that the local environment and the availability of nuclei influences the distribution and finish of particles the most.

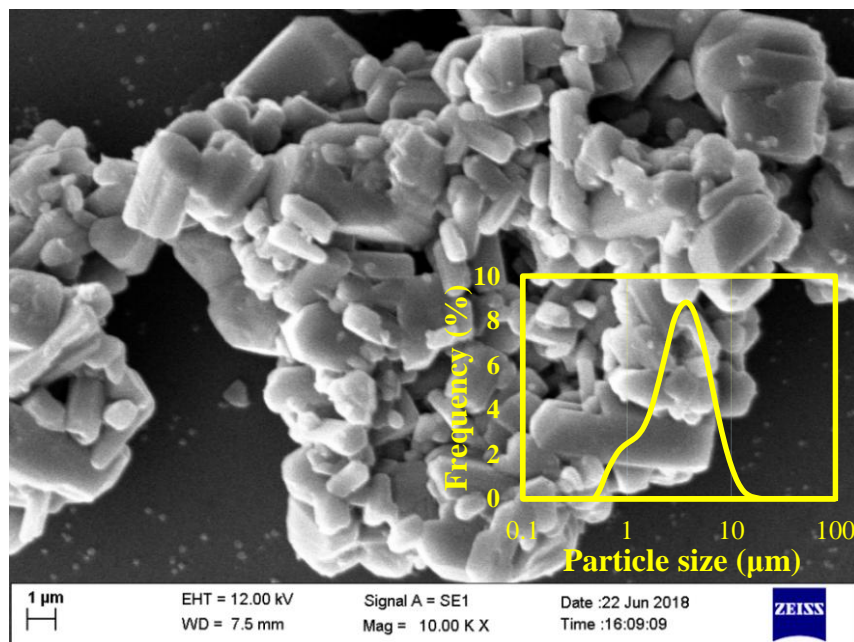


Fig. 6.18: FESEM image of zinc oxalate
(Zn=2.73 g/L, t=3 hr, oxalic acid concentration=1M)

Image of the particles after 3h of stripping time are shown in Figure 6.18. Plate type particles of different sizes are seen clustered together, they are not attached but held together therefore, the PSD (Figure 6.18 inset) doesn't show any tendency of agglomeration. Smaller sized particles in the distribution are the ones that are precipitated late.

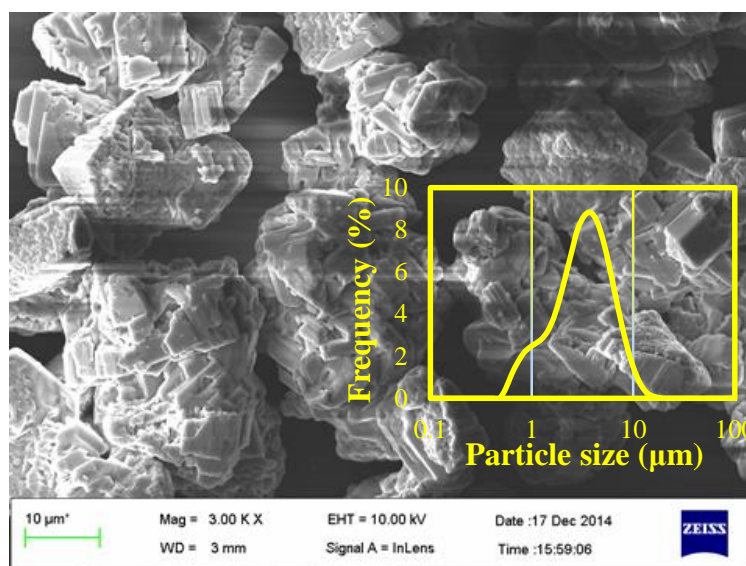


Fig. 6.19: FESEM image of zinc oxalate
(Zn=2.73 g/L, t=3 hr, oxalic acid concentration=0.114M)

Precipitation of zinc oxalate without substantial excess of oxalic acid (0.114M) after 3 hr contact leads to evolution of irregular shaped structures (Figure 6.19) that are built from rectangular shaped sheets which shows tendency to agglomerate although, the agglomerates were not identified in the PSD (Figure 6.19 inset)

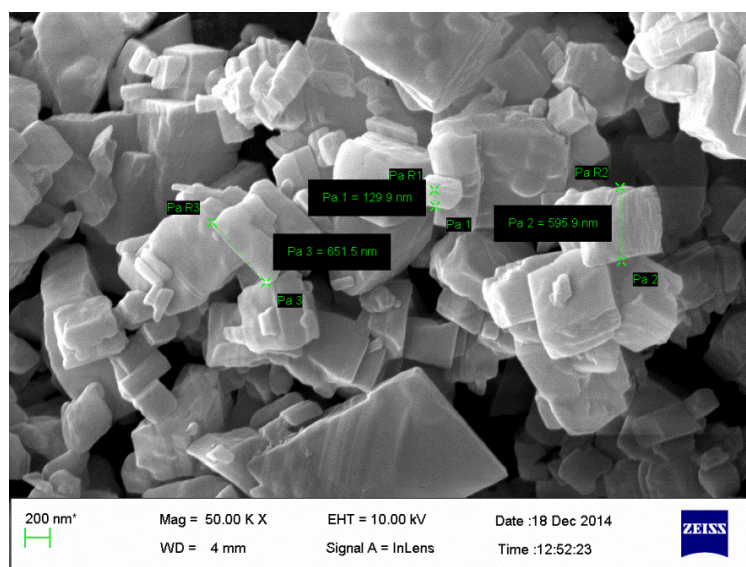
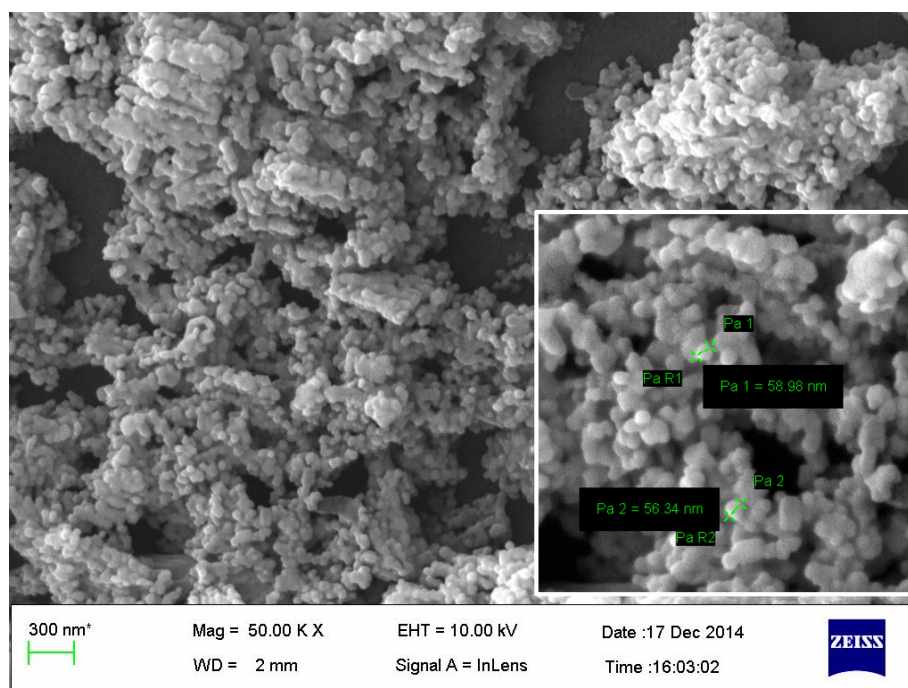


Fig. 6.20: FESEM of zinc oxalate
(Zn=9.72g/L, t=3 hr, oxalic acid concentration= 1M)

Precipitation for 3 h at high zinc concentration (9.72g/L) in the solution led to well defined rectangular particles (Figure 6.20) over a wide size range. This was a case of abundant supply of nuclei that led to formation and finishing of the particles formed. The smaller sized particles seem to have appeared in the later times of precipitation, even PSD suggests such pattern.

The FESEM image of zinc oxide obtained from the oxalate precipitated with 0.114 M oxalic acid, at 150 rpm, 3 hr duration and initial zinc concentration of 2.7 g/L is shown in Figure 6.21



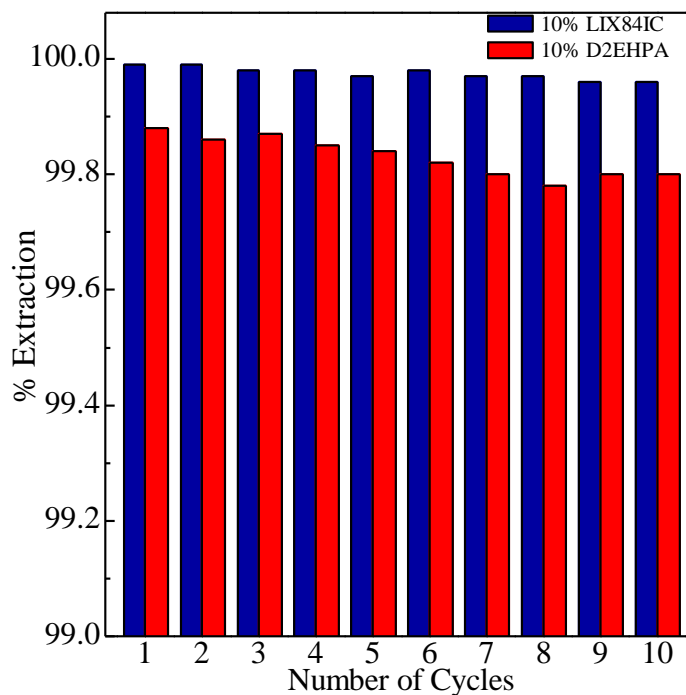
6.21 FESEM of zinc oxide

(Zn=2.73 g/L, t=3 hr, oxalic acid concentration= 0.114M)

The FESEM of the oxalate under same conditions is shown in Fig 6.19. Comparing Figure 6.19 and Figure 6.21 it can be seen that oxalate on transformation to the oxide did not lose its ordered structure.

6.3.7 Recyclability of extractant

After extraction and stripping in a single stage the extractants were further stripped with sulfuric acid to strip off any residual metal in the organic phase for reuse. It can be seen that both the extractants could be used for ten cycles without any substantial decline in their extraction ability (Figure 6.22).



6.22 Recyclability of extractants

6.4 Antimicrobial properties of copper oxide and zinc oxide

Antimicrobial activity of metal oxide particles has largely been studied with gram negative bacteria *Escherichia coli* and gram positive *Staphylococcus aureus*. These microbes are known to be sensitive to both ZnO and CuO particles. (Pasquet *et al.*, 2014, Ameer *et al.*, 2012).

A bioassay was performed against four gram negative bacteria *Escherichia coli* (ATCC 27853), *Pseudomonas aeruginosa* (ATCC 25922), *Shigella flexneri* (ATCC 12022), *Salmonella typhimurium* (ATCC 14028), and one gram positive representative *Staphylococcus aureus* (ATCC 25923) strains.

Kirby-Bauer disc diffusion method (Biemer, 1973) used for testing antibiotic susceptibility was performed for antibacterial test where, KBr discs containing copper oxide/zinc oxide particles were placed instead of antibiotic discs. Copper oxide/zinc oxide particles were mixed with Potassium Bromide (KBr) (0.15 gm) in a mortar pestle. The prepared mixture was pressed on a standard KBr press for 2 minutes to form a disc 11.2 mm in diameter. Control was prepared without the addition of the metal oxide powder and contained only KBr.

Nutrient Broth (NB) (2.5 % w/v Nutrient Broth Medium in DW, MM244, Hi Media,

Mumbai), soft agar (0.8% Agar Agar in DW, GRM666, Hi Media, Mumbai) and Nutrient Agar (NA) (2.5% NB and 2.0% Agar Agar type-I in DW) were sterilized by autoclaving at 15 lbs pressure (121°C) for 15 minutes. The bacterial cultures were grown overnight in NB. From this overnight grown culture 200 µL was seeded individually in 5 ml of 0.8% soft agar, thoroughly mixed and layered over the preset NA containing Petri plates and allowed to solidify. Once the soft agar layer solidified, the prepared KBr discs were kept on the agar surface. The plates were incubated at 37 °C for 24 hours and the diameter of growth inhibition was measured. The experiment was performed under aseptic conditions.

KBr discs containing 250, 500, 1000, 1500 µg CuO and ZnO were used to determine the lowest bacterial concentration required to prevent the growth of the bacteria. Tests were conducted using *Staphylococcus aureus* and *Escherichia coli*. Discs with KBr alone did not show any zone of inhibition suggesting that KBr showed no antibacterial activity. Minimum bacterial concentration was 500 µm for both the bacteria studied for both copper and zinc oxide. Increase in concentration of CuO and ZnO resulted in an increase of the inhibition zone. Concentrations beyond 1000 µg did not affect the zone of inhibition. Hence, all the experiments with other bacteria were carried out with 1000 µg of CuO and ZnO.

Antimicrobial activity of the synthesized CuO and ZnO were performed using 1000 µg of each of the oxides. Four Gram-negative bacteria *Escherichia coli*, *Pseudomonas aeruginosa*, *Shigella flexneri* and *Salmonella typhimurium* and one Gram-positive gram positive *Staphylococcus aureus* were used. Figure 6.23 and Figure 6.24 show the zone of inhibition observed for copper oxide and zinc oxide particles against the bacterial strains. Both copper oxide and zinc oxide demonstrated antibacterial activity against all the five bacteria tested. The radial diameter of the zone of inhibition observed is given below.

Organisms	CuO ZOI(mm)	ZnO ZOI(mm)
<i>Escherichia Coli</i>	16	20
<i>Pseudomonas Aeruginosa</i>	20	18
<i>Shigella Fexneri</i>	30	18
<i>Salmonella Typhimurium</i>	29	20
<i>Staphylococcus Aureus</i>	31	23

The diameter of the inhibition zone which reflects the susceptibility of the microorganism was higher for copper oxide in comparison to zinc oxide. Copper oxide exhibited maximum bacterial growth inhibition (31 mm) against *Staphylococcus aureus*.

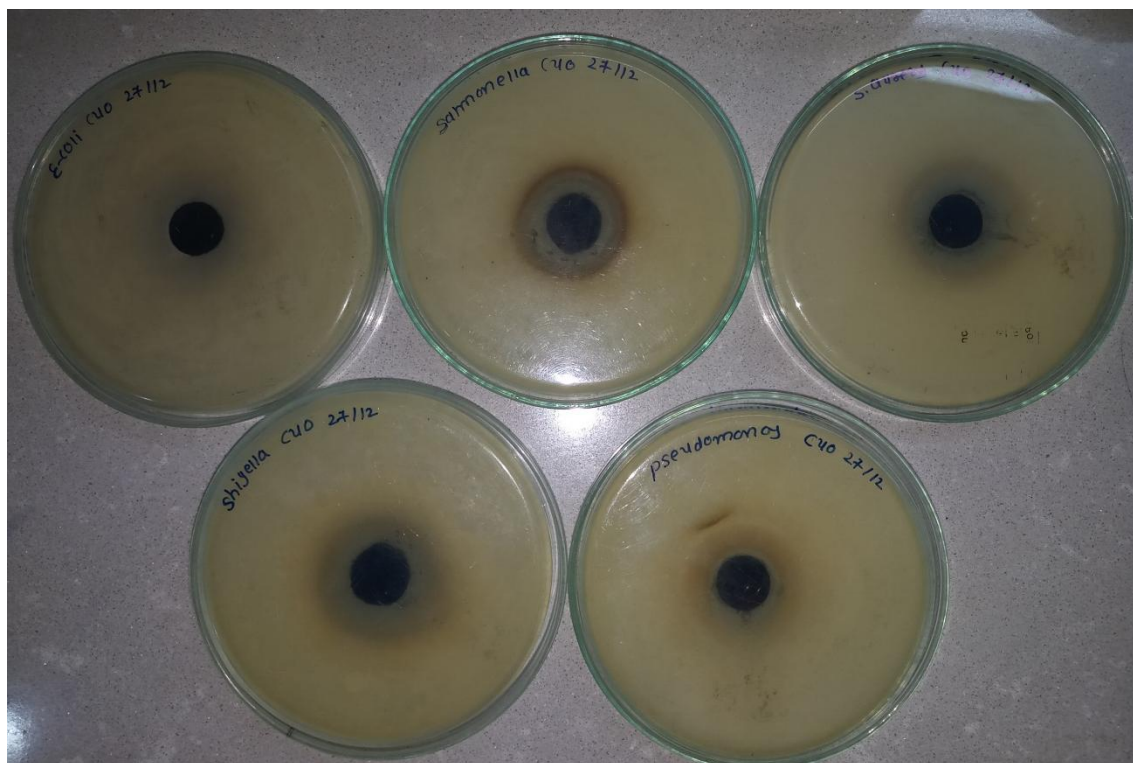


Fig. 6.23: Bactericidal activity of CuO on *Escherichia coli*, *Pseudomonas aeruginosa*, *Shigella flexneri* *Salmonella typhimurium* and *Staphylococcus aureus*

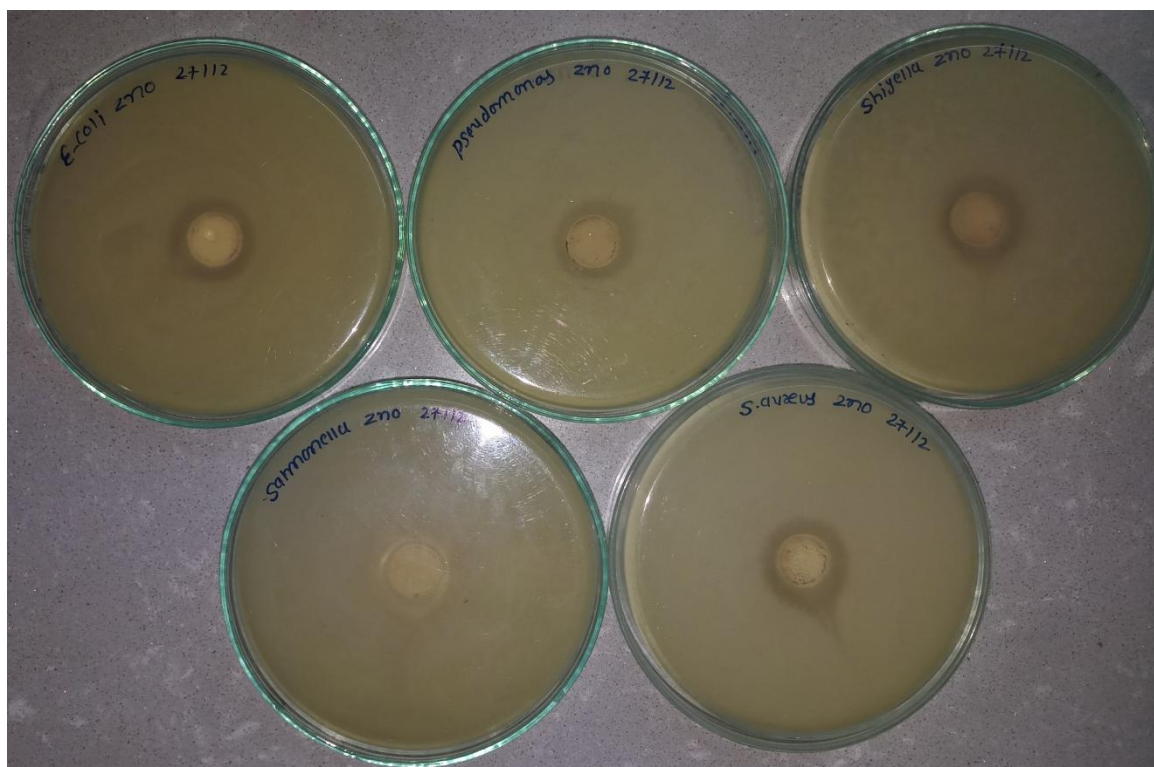


Fig. 6.24: Bactericidal activity of ZnO on *Escherichia coli*, *Pseudomonas aeruginosa*, *Shigella flexneri* *Salmonella typhimurium* and *Staphylococcus aureus*

Based on these results, it could be concluded that CuO and ZnO obtained in this investigation have significant antibacterial action on both of the Gram classes of bacteria. The current investigation of antimicrobial activity of copper oxide and zinc oxide was only cursory and explorative a more robust investigation would yield greater insight with reference to the influence of particle size, morphology and elucidate the mechanism of antibacterial activity.

6.5 Conclusions

Brass rinse liquors were used to recover copper and zinc on the same lines as brass pickle liquors were used for recovery of these metals. As expected the concentration of the metals in the rinse solution were significantly lower than the concentration of metals in the brass pickle liquor. In view of this the extraction circuits were designed to recover copper using 10% (v/v) LIX 84-IC and subsequently zinc was recovered using 10% (v/v) D2EHPA. The recovery was quantitative (99.9) and 98.8% zinc was recovered at an equilibrium pH of 2.5 for Cu and 3 for zinc.

The metal values were recovered by PS that regenerated the solvent for reuse. The efficacy of PS was explored over a wide range of parametric space and the nature of the particles obtained under different precipitating conditions was investigated. Key parameters varied were rate of agitation, precipitation time, concentration of oxalic acid and initial metal concentration. For all these situations the PSD were obtained and an attempt is made to interpret the precipitation patterns.

Some significant findings are:

Stripping mechanism of copper from LIX 84-IC and zinc from D2EHPA loaded organic phase are significantly different since copper is held as a chelate while zinc is solubilized by D2EHPA. Hence precipitation of particles in Cu-LIX 84-IC system will take place at the interface while D2EHPA because of its phase transfer behavior takes place in the aqueous film surrounding the oil phase as a result copper stripping though is much better defined than the stripping of zinc. However, in both the cases the precipitation yield consistently increases with concentration of acid. Increase in degree of agitation and contact time, the PSD narrows and there is a shift towards smaller sizes and more stable size distribution patterns emerge.

The effect of concentration of oxalic acid on copper stripping is not very pronounced although there are differences in particle sizes when oxalic acid concentration is changed from 0.078 to 1M. For the case of zinc oxalate there is a drastic reduction in particle size with increase in oxalic acid concentration. The $D_{0.5}$ shifts from 18.26 μm at 0.057M to 3.07 μm at 1M concentration.

A four to five fold increase in concentration of the metal in the organic phase does not make any significant difference in the PSD obtained.

The particles obtained were characterized by XRD, FTIR, EDX and XRF studies and pure copper and zinc oxalate were obtained. Morphology of the copper oxalate particles were cushion shaped whereas zinc oxalate particles had sharp edges which were built layer by layer. Controlled calcinations of the oxalate particles at the appropriate temperatures resulted in the formation of copper and zinc oxide. The oxalates on transformation to the oxide did not lose its ordered structure. XRD analysis revealed that pure copper oxide and zinc oxide were obtained. For both copper and zinc oxide the metal- oxygen ratios were in stoichiometric proportions.

The antibacterial activity of copper oxide and zinc oxide were evaluated against four gram negative and one gram positive bacteria. Both the oxides exhibited antibacterial activity when tested against the five organisms. The diameter of the inhibition zone which reflects the susceptibility of the microorganism was higher for copper oxide.

References

- Ameer Azam A, Ahmed A, Oves M, Khan M, Habib S, Memic A. Antimicrobial activity of metal oxide nanoparticles against Gram-positive and Gram-negative bacteria: a comparative study. *Int J Nanomedicine*. 2012; 7: 6003–6009.
- Biemer JJ. Antimicrobial susceptibility testing by the Kirby-Bauer disc diffusion method. *Ann Clin Lab Sci*. 1973; 3(2): 135-140.
- Campbell DP. Precipitation of Enriched Lutetium by Direct Oxalate Extraction. Trace: *Tennessee Research and Creative Exchange*, University of Tennessee Honors Thesis Projects. 1999.

- Combes E, Sella C, Bauer D, Sabot JL. A study of the formation of acid and neutral yttrium oxalate powders from precipitation-stripping reaction in a Lewis-type cell. *Hydrometallurgy*. 1997; 46: 137-148.
- Deferm C, Van De, Voorde M, Luyten J, Oosterhof H, Fransaeer J, Binnemans K. Purification of indium by solvent extraction with undiluted ionic liquids. *Green Chem*. 2016; 18(14): 4116-4127.
- El-Hefny NE. Chemical kinetics and reaction mechanisms in solvent extraction: New trends and applications. *J PhysSci*. 2017; 28(281): 129-156.
- Elliott HA, Herzig LM. Oxalate Extraction of Pb and Zn from Polluted Soils : Solubility limitations oxalate extraction of Pb and Zn from polluted soils : Solubility limitations. *J SoilCont*. 2010; 8 (1999,1): 105-116.
- Hirai T, Kobayashi J, Komasaawa I. Preparation of acicular ferrite fine particles using an emulsion liquid membrane system. *Langmuir*. 1999; 15: 6291–6298.
- Hirai T, Nagaoka K, Okamoto N, Komasaawa I. Preparation of copper oxalate fine particles using emulsion liquid membrane system, *J ChemEngJpn*. 1996; 29: 842–850.
- Hirai T, Okamoto N, Komasaawa I. Preparation of spherical oxalate particles of rare earths in emulsion liquid membrane system. *AIChE J*. 1998; 44: 197–206.
- Huang T, Juang R. Kinetics and mechanism of zinc extraction from sulfate medium with Di(2-ethylhexyl) phosphoric acid. *J ChemEngJpn*. 1986; 19: 379-386.
- Iglesias M, Antico E, Salvado V, Masana A, Valiente M. Effect of Y(III) distribution between aqueous nitrate and organic D2EHPA solutions on the Y(III) precipitation stripping using oxalic acid. *Solvent Extr Ion Exch*. 1999; 17(2): 277-300.
- Konishi Y, Asai S, Murai T. Precipitation stripping of neodymium from carboxylate extractant with aqueous oxalic acid solutions. *Ind Eng Chem Res*. 1993; 32(5): 937-942.
- Konishi Y, Asai S, Murai T. Precipitation stripping of neodymium from carboxylate extractant with aqueous oxalic acid solutions. *Ind Eng Chem Res*. 1993; 32(5): 937-942.
- Konishi Y, Noda Y, Asai S. Precipitation stripping of yttrium oxalate powders from yttrium-loaded carboxylate solutions with aqueous oxalic acid solutions. *IndEngChem Res*. 1998; 37: 2093-2098.

- Konishi Y, Noda Y. Precipitation stripping of rare-earth carbonate powders from rare-earth-loaded carboxylate solutions using carbon dioxide and water. *IndEngChem Res.* 2001; 40(8): 1793-1797.
- Konishi Y. Precipitation stripping of yttrium oxalate powders from yttrium-loaded carboxylate solutions with aqueous oxalic acid solutions. *IndEngChem Res.* 1998; 37(6): 2093-2098.
- Lee K, Kim J, Jang J. Recovery of zinc in spent pickling solution with oxalic acid. *Korean Chem Eng Res.* 2017; 55(6): 785-790.
- Qiu S, Dong J, Chen G. Preparation of Cu nanoparticles from water-in-oil microemulsion. *Colloid Interface Sci.* 1999; 216: 230–234.
- Pasquet J, Chevalier Y, Pelletier J, Couval E, Bouvier D, Bolzinger M. The contribution of zinc ions to the antimicrobial activity of zinc oxide. *Colloids and Surfaces A: Physicochem Eng Aspects.* 2014; 457: 263–274.
- Ropp RS, Kastl L, Furst A. Biochemical and behavioural effects of some substituted catechols. *Arch. Int. Pharmacodyn Ther.* 1969; 181: 127-132.
- Sanuki, S, Sugiyama, A, Tunekawa, M, Kadomachi K, Arai K. Precipitation stripping of samarium oxalate from organic solution containing acid type extractant by oxalic acid. *J JapanInst Metals.* 1994; 58: 1271-1278.
- Sengupta B, Tamboli CA, Sengupta R. Synthesis of nickel oxalate particles in the confined internal droplets of w/o emulsions and in systems without space confinement. *ChemEng J.* 2011; 169: 379–389.
- Shter GE, Grader GS. YBCO Oxalate coprecipitation in alcoholic solutions. *J Am Ceram Soc.* 1994; 77(6): 1436-1440.
- Sinha MK, Pramanik S, Sahu SK, Prasad LB, Jha MK, Pandey BD. Development of an efficient process for the recovery of zinc and iron as value added products from the waste chloride solution. *Sep Purif Technol.* 2016; 167(July): 37-44.
- Smith PM. High-purity rare earth oxides produced via precipitation stripping. *Metall Mater Trans B.* 2007; 38(5): 763-768.
- Soare LC, Bowen P, Lemaitre J, Hofmann H. Precipitation of nanostructured copper oxalate: Substructure and growth mechanism, *J PhysChem B.* 2006; 110: 17763–17771.

- Wang Z, Ding F, Zhan J, Zhang C. Solvent extraction mechanism and precipitation stripping of bismuth(III) in hydrochloric acid medium by tributyl phosphate. *J Cent South Univ.* 2016; 23(12): 3085-3091.
- Wan M, Jin D, Feng R, Si L, Gao M, Yue L. Pillow-shaped porous CuO as anode material for lithium-ion batteries. *InorgChemCommun.* 2011; 14: 38-41.
- Wojciechowska A, Wieszczycka K, Wojciechowska I. Selective recovery of Zn(II) from multimetal acidic chloride solution with hydrophobic pyridine derivatives. In: *ISEC 2017 - The 21st International Solvent Extraction Conference.* 2017; 2: 146-152.
- Zhang Y, Zhu W, He H, Zheng A. Synthesis of lanthanum oxalate hierarchical micro-particles and nano-tubes. *J ExpNanosci.* 2014; 9(8): 851-859.
- Zhu P, Chen Y, Fen ZY, Qian GR. Preparation of ultrafine copper oxide using metal powders recovered from waste printed circuit boards. *J Hazardous, Toxic, and Radioactive Waste.* 2013; 17(3): 175-180.
- Zielinski S, Buca M, Famulski M. Precipitation stripping processes for heavy metals. *Hydrometallurgy.* 1998; 48: 253–263
- Zielinski S, Buca M, Szczepanik A. Precipitation stripping of lanthanum and neodymium. *Hydrometallurgy.* 1991; 26(2): 243-254.
- Zielinski S, Szczepanik A. Selective precipitation stripping process for lanthanides. *Hydrometallurgy.* 1993; 33(1-2): 219-226.